

A simple continuum model for boron clustering based on atomistic calculations

Srinivasan Chakravarthi^{a)}

Department of Manufacturing Engineering, Boston University, Boston, Massachusetts 02215

Scott T. Dunham

Department of Electrical Engineering, University of Washington, Seattle, Washington 98195

(Received 10 November 1999; accepted for publication 11 January 2001)

Boron exhibits anomalous diffusion during the initial phases of ion implant annealing. Boron transient enhanced diffusion is characterized by enhanced tail diffusion coupled with an electrically inactive immobile peak. The immobile peak is due to clustering of boron in the presence of excess interstitials which also enhance boron diffusion in the tail region. We present a simple model for the formation of immobile boron interstitial clusters and associated point defect interactions derived based on atomistic calculations. © 2001 American Institute of Physics.

[DOI: 10.1063/1.1352576]

I. INTRODUCTION

It is well known that ion implantation introduces damage that on annealing leads to the phenomenon of transient enhanced diffusion (TED).^{1,2} Implantation introduces a large number of point defects orders of magnitude higher than the implanted dopant concentration. These excess interstitials and vacancies recombine with each other during the initial stages of annealing. The remaining point defects interact with the dopants via coupled diffusion.³⁻⁶ Excess point defects also form extended defects. For subamorphizing implants, interstitials primarily form {311} defects.⁷⁻⁹ However, larger implant doses/energies lead to the formation of dislocation loops.^{10,11} Under TED conditions, boron is found to be immobilized at concentrations well below solid solubility.¹² This has been explained on the basis of the formation of boron interstitial clusters (BICs). Models using either a moment-based approach¹³ or a discrete set of cluster compositions^{14,15} have been successfully used for modeling of boron interstitial clusters. A problem with both of these approaches is that they lead to complicated models with associated long simulation times and large sets of nonunique parameters. In previous work,¹⁶ we derived a simple cluster model for BICs from a multicluster model¹⁵ based on *ab initio* calculations performed at Lawrence Livermore National Labs.¹⁷ Despite its simplicity, the model accurately describes boron clustering and anomalous diffusion behavior and replicates a much more complicated model. However, both the multicluster model¹⁷ and the simple model¹⁶ do not include cluster charge states. To be physically consistent, it is necessary to include charge exchange reactions involved in the electrical deactivation of boron via clustering. In this article, we describe the methodology used to identify the dominant cluster species and rate limiting processes. We use this information to develop a simple model, then further extend this model to include cluster charge states.

II. MULTICLUSTER MODELS FOR BORON TED

Boron/interstitial aggregation is a complicated process as there is a huge array of potential cluster compositions. In previous work, Caturla *et al.*¹⁷ and Lilak *et al.*¹⁵ presented boron clustering models based on the same calculations which we use in this work. Pelaz *et al.*¹⁴ derived a similar model, but with a somewhat different parameter set. In each case, they considered a large range of clusters such as shown in Fig. 1, with an associated large set of continuity equations and parameters.

The model implemented in this work uses kinetic reactions that lead to the formation of clusters. For reactions of the form $A+B \rightleftharpoons AB$, the rate of formation of AB is given by

$$R_{AB} = 4\pi r_{\text{cap}}(D_A + D_B) \left(C_A C_B - \frac{C_{AB}}{K_{\text{eq}}} \right), \quad (1)$$

where r_{cap} is the capture radius of the reaction and D and C represent diffusivity and concentration. K_{eq} is the equilibrium constant which for dilute solutions is given by

$$K_{\text{eq}} = \frac{1}{C_{\text{Si}}} \exp\left(\frac{E_B}{kT}\right). \quad (2)$$

C_{Si} is the number of available lattice sites in silicon ($\sim 5 \times 10^{22} \text{ cm}^{-3}$), and E_B is the binding energy between A and B. As shown in Fig. 1, each cluster can grow/dissolve by the addition/release of a silicon self-interstitial or boron interstitial. For example, a substitutional boron can react with a boron interstitial to form an immobile B_2I which can further react with another interstitial to form a B_2I_2 cluster or with a mobile interstitial boron (B_i) to give B_3I_2 . There are thus two possible sets of reactions



with associated rates given by the equations

^{a)}Currently at: Silicon Technology Development, Texas Instruments, Dallas, TX 75243; electronic mail: s-chakravarthi@ti.com

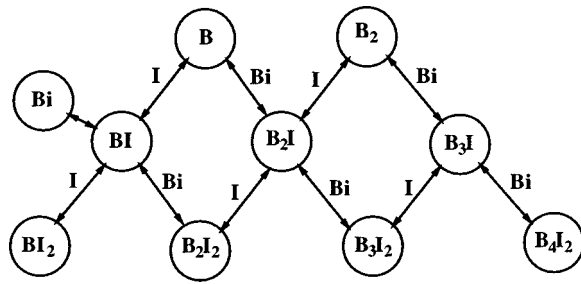


FIG. 1. Cluster reactions considered in the full model as given by *ab initio* calculations (Ref. 17).

$$R_{B_n I_m / I} = 4 \pi r_{cap} D_I \left(C_{B_n I_m} C_I - \frac{C_{B_n I_{m+1}}}{K_{B_n I_m / I}} \right), \quad (5)$$

$$R_{B_n I_m / B_i} = 4 \pi r_{cap} D_{B_i} \left(C_{B_n I_m} C_{B_i} - \frac{C_{B_{n+1} I_{m+1}}}{K_{B_n I_m / B_i}} \right). \quad (6)$$

Cluster energetics calculations from Caturla *et al.*¹⁷ were used as the basis for the simulations, with ten different clusters considered: BI, BI₂, B₂I, B₂I₂, B₃I, B₃I₂, B₄I₂, B₂, B₃. The cluster energies used in the simulation are tabulated in Table I. It should be noted that using dissociation energies from Caturla *et al.*¹⁷ and following different pathways for the formation of B₂I and B₂I₂ from B and I yields different binding energies. Hence, an intermediate energy was chosen. This choice does not change the relative stability of clusters.

The large binding energies for the formation of B₃I suggests the importance of B₃I clusters. However, it is necessary to look at the kinetics and energetics of all these processes to identify the number of equations and cluster concentrations that need to be solved to model this system. For example, interstitial rich clusters may be more important in the presence of the higher interstitial supersaturations typical of the very early stages of annealing. The diffusivity of the boron interstitial can be calculated from the equilibrium boron diffusivity¹⁸ combined with the B and Bi binding energy (Table I). Table II shows the point defect parameters used.^{19–22} All simulations assume a “+1 model” for interstitials following implantation.²³

TABLE I. Cluster energetics based on atomistic calculations (Ref. 17) used for the full system.

Reaction	Binding energy (eV)
B + I ⇒ BI	1.0
B + I ⇒ B _i	0.7
B _i + B ⇒ B ₂ I	1.3
B ₂ + I ⇒ B ₂ I	1.6
B ₂ I + I ⇒ B ₂ I ₂	1.2
BI + B _i ⇒ B ₂ I ₂	1.5
BI + I ⇒ BI ₂	1.4
B ₃ + I ⇒ B ₃ I	3.3
B ₂ + B _i ⇒ B ₃ I	2.8
B ₂ I + B _i ⇒ B ₃ I ₂	-0.1
B ₃ I + I ⇒ B ₃ I ₂	-1.3
B ₃ I + B _i ⇒ B ₄ I ₂	1.5

TABLE II. Point defect parameters used for the simulations.

Parameter	Pre-exponent	Energy (eV)	Ref.
D _V (cm ² /s)	1 × 10 ⁻³	0.43	19
D _V C _V [*] (cm ⁻¹ s ⁻¹)	6.95 × 10 ²¹	3.88	20
D _I (cm ² /s)	0.158	1.37	21
D _I C _I [*] (cm ⁻¹ s ⁻¹)	1.5 × 10 ²⁶	4.95	22
K _{I+}	5.68	0.26	31
D _{B⁰} (cm ² /s)	0.3	3.57	18
D _{B+} (cm ² /s)	1.8	3.57	18
r _{cap} (nm)	0.27	0	

A. Kinetics

We first look at the kinetics of the different processes. Concentrations of clusters that are in dynamic equilibrium with the free interstitial and boron concentrations can be expressed as simple analytic expressions (e.g., C_{B_nI_m} = K_{B_nI_m} C_Bⁿ C_I^m). Figure 2 shows the time evolution of cluster concentrations normalized by their equilibrium value (C_{B_nI_m} / K_{B_nI_m} C_Bⁿ C_I^m) for each cluster species. A value of “1” indicates that the system is in dynamic equilibrium with the free B and I. These normalized values are calculated at the peak of the implant profile. Our analysis of this system finds that most of the clusters rapidly achieve dynamic equilibrium with the free boron and interstitial concentrations, suggesting the possibility of reducing the number of equations and parameters needed to describe the system. As shown in Fig. 2, except for B₃I and B₄I₂, all the clusters reach dynamic equilibrium with the B and I concentrations within 0.1 s. B₃I and B₄I₂ are also in local dynamic equilibrium with each other as demonstrated by their overlapping curves in Fig. 2.

B. Energetics

We next identify the most stable clusters for interstitial supersaturations characteristic of different annealing times. Figure 3(a) shows the equilibrium concentrations of the clusters under conditions typical of the period before {311} defects form. For high interstitial supersaturations representative of very short times (<1 s), BI₂ can be present in significant numbers. This helps to immobilize boron atoms initially. Note that the strong clustering keeps the free B and thus the B₂I₂ concentration low, and at such short times the

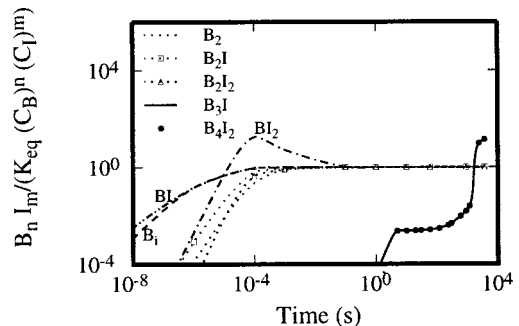


FIG. 2. Simulations using the full cluster model of normalized cluster concentrations (relative to their equilibrium value) versus time for an 800 °C anneal. Note that the curves for B₃I and B₄I₂ overlap.

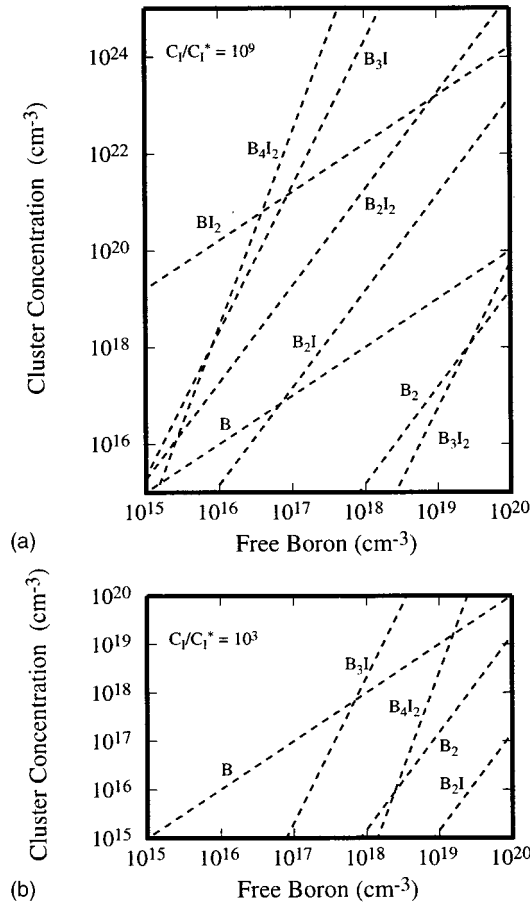


FIG. 3. Equilibrium cluster concentrations ($K_{B_n I_m} C_B^n C_I^m$) vs free boron concentration at 800 °C for free interstitial concentrations of (a) $10^9 C_I^*$ characteristic of very early stages of TED, and (b) $10^3 C_I^*$ typical of TED conditions in the presence of {311} defects. Initially, BI_2 is the primary cluster and helps immobilize the boron, while B_3I is the primary cluster during most of the anneal.

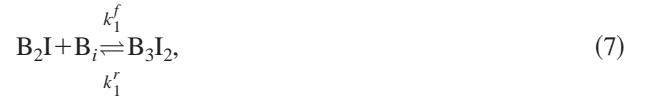
B_3I and B_4I_2 concentrations are far below their equilibrium values due to the slower formation rate of B_3I (Fig. 2). Once {311} defects form, the interstitial concentration drops. For typical TED supersaturations ($C_I/C_I^* \sim 10^3$), the dominant species is B_3I , as shown in Fig. 3(b).

III. SIMPLE CLUSTER MODEL

The following conclusions can be made from the above analysis:

- (i) The concentration of all the small clusters rapidly equilibrate with the free B and I concentrations.
- (ii) At short times, BI_2 is the dominant cluster.
- (iii) At longer times, B_3I is the dominant cluster and needs to be solved numerically since it is present in non-equilibrium quantities.

Based on the above observations, we can simplify the system of immobile clusters from ten to that of just B_3I . Since B_3I forms via the unstable cluster B_3I_2 (Ref. 17) the reactions



can be combined to give a net formation rate for B_3I :

$$R_{B_3I} = k_{B_3I}^{\text{eff}} \left(C_{B_2I} C_{B_i} - \frac{C_{B_3I} C_I}{K_{B_3I}} \right), \quad (9)$$

$$K_{B_3I} = \frac{k_1^f k_2^f}{k_1^r k_2^r} = \exp\left(\frac{-0.1 \text{ eV} + 1.3 \text{ eV}}{kT}\right), \quad (10)$$

using values from Table I.

$$k_{B_3I}^{\text{eff}} = k_1^f \left(\frac{k_2^f}{k_1^r + k_2^r} \right) = \left[\frac{k_1^f}{1 + k_1^f / (k_2^r K_{B_3I})} \right], \quad (11)$$

where $k_2^f / (k_1^r + k_2^r)$ represents the probability that B_3I_2 will dissociate into $B_3I + I$ rather than $B_2I + B_i$. Since the small clusters are in dynamic equilibrium

$$C_{B_2I} = K_{B_2I} C_B C_{B_i}, \quad (12)$$

k_1^f and k_2^r are assumed to be diffusion limited and are hence,

$$k_1^f = 4 \pi r_{\text{cap}} D_{B_i}, \quad (13)$$

$$k_2^r = 4 \pi r_{\text{cap}} D_I. \quad (14)$$

As BI_2 is the dominant cluster at short times [see Fig. 3(a)], we can neglect the other small clusters. Since BI_2 reaches local equilibrium quickly (see Fig. 2), we can approximate the BI_2 concentration by an analytic function of the B and I concentrations ($C_{BI_2} = K_{BI_2} C_B C_I^2$). However, adding the rate equation for BI_2 is actually easier to implement and requires minimal computational overhead. A two-moment model was used for modeling interstitial defects ({311} defects and dislocation loops). This model was characterized^{24,25} based on interstitial evaporation rates obtained from quantitative transmission electron microscopy (TEM). Using the same energies from Table I for both models, we compared our simplified model to the full system and found that the results are virtually indistinguishable. Figure 4 shows an example of this comparison as well as data from Intel²⁶ for TED at 800 °C for a $2 \times 10^{14} \text{ cm}^{-2}$, 40 keV implant. Similar agreement was obtained at higher and lower temperatures (700 and 900 °C) as well as for other implant energies.

Based on the fact that B clustering is not seen for oxidation enhanced diffusion (OED) experiments, Pelaz *et al.*²⁷ suggest boron clusters must form via a more interstitial rich pathway. However, we find it is not necessary to include an interstitial rich pathway to be consistent with OED experiments. For example, Fig. 5 shows a simulation of a delta doped boron layer under OED at 790 °C with a surface interstitial supersaturation of 30. No significant clustering is predicted by the model consistent with experimental observation.²⁸

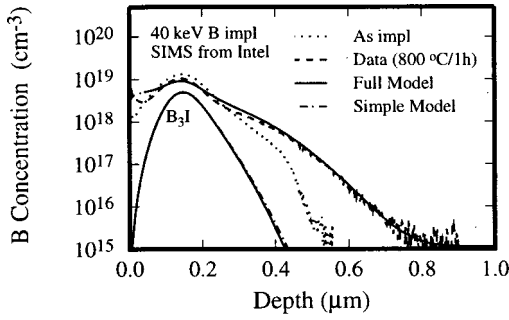


FIG. 4. Comparison of full model with the simplified model for a 40 keV $2 \times 10^{14} \text{ cm}^{-2}$ B implant annealed at 800 °C for 1 h. Also shown for comparison are secondary ion mass spectrometry (SIMS) data from Intel (Ref. 26). Note that the full model and simple model show indistinguishable final profiles. The B_3I concentrations for the two models are also nearly identical.

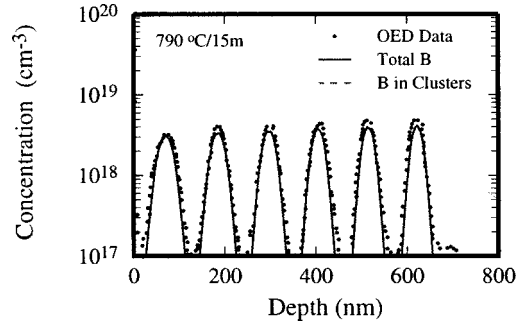
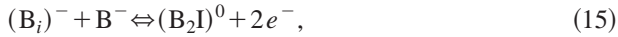


FIG. 5. SIMS profiles for a B-doped superlattice after 790 °C anneal for 15 min in an oxidizing ambient, shown along with the simulation results (data from Ref. 28). Simulations show no clustering of boron under the relatively low interstitial injection conditions typical of OED ($C_1/C_1^* \sim 30$). This is in agreement with experimental observations that moderately doped boron marker layers do not trap interstitials during OED experiments.

IV. EXTENSION TO CHARGE STATES

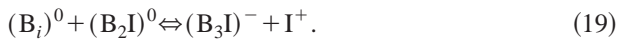
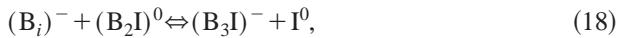
The cluster models considered in earlier sections did not include charge states for the various clusters. However, since clustering involves deactivation and formation of clusters of different charges, it is necessary to include cluster charge states to be physically consistent. We have extended our model based on charged defect calculations from Lenosky *et al.*²⁹ which conclude that the dominant charge states of the clusters we have identified as critical to modeling are $(BI_2)^+$, $(B_2I)^0$, and $(B_3I)^-$. The boron diffusion model is based on recent *ab initio* calculations.³⁰ Clustering proceeds as



Since $(B_2I)^0$ quickly reaches dynamic equilibrium with B and B_i ,

$$C_{(B_2I)^0} = K_{(B_2I)^0}^{eq} C_B C_{(B_i)^-} \left(\frac{p}{n_i} \right)^2. \quad (17)$$

$(B_3I)^-$ formation can proceed by a reaction with B_i which has either a net negative $(B_i)^-$ or neutral $(B_i)^0$ charge. Hence, we can write



It should be noted that under extrinsic conditions, diffusion via $(B_i)^0$ dominates ($D_B \propto p/n_i$), so Eq. (19) is the dominant pathway. The reaction rates given by Eqs. (18) and (19) are

$$R_{(B_i)^-/B_2I} = k_{B_i^-/B_2I} \left[C_{(B_i)^-} C_{(B_2I)^0} - \frac{C_{(B_3I)^-} C_{I^0}}{K_{(B_i)^-/B_2I}} \right], \quad (20)$$

$$R_{(B_i)^0/B_2I} = k_{B_i^0/B_2I} \left[C_{(B_i)^0} C_{(B_2I)^0} - \frac{C_{(B_3I)^-} C_{I^+}}{K_{(B_i)^0/B_2I}} \right]. \quad (21)$$

Assuming ionization reactions are fast and that diffusivities are independent of charge state [$D_{(B_i)^-} = D_{(B_i)^0}$ and $D_{I^0} = D_{I^+}$], we can write the equilibrium constants for Eqs. (20)

and (21) in terms of the Fermi level dependent boron diffusivities available from equilibrium experiments¹⁸ (D_B^+ and D_B^0)

$$\frac{K_{(B_i)^-/B_2I}}{K_{(B_i)^0/B_2I}} = \frac{C_{(B_i)^0}}{C_{(B_i)^-}} \frac{C_{I^0}}{C_{I^+}} = \frac{D_B^+}{D_B^0 K_{I^+}}, \quad (22)$$

where K_{I^+} accounts for the Fermi level dependence of interstitial concentration³¹ and is defined such that

$$C_{I^+} = K_{I^+} C_{I^0} \left(\frac{p}{n_i} \right). \quad (23)$$

The total rate of formation of $(B_3I)^-$ is then

$$R_{(B_i)/B_2I} = (k_{B_i^-/B_2I}^{eff} + k_{B_i^0/B_2I}^{eff}) \times \left[C_{(B_i)^-} C_{(B_2I)^0} - \frac{C_{(B_3I)^-} C_{I^0}}{K_{(B_i)^-/B_2I}} \right], \quad (24)$$

where $K_{(B_i)^-/B_2I}$ is the equilibrium constant defined for Eq. (20) with

$$k_{B_i^-/B_2I}^{eff} = \left(\frac{4 \pi r_{cap} D_B^0}{K_{B_i^-/B_2I} C_{I^0}^* (1 + \gamma_{B_i^-/B_2I}^{eff})} \right), \quad (25)$$

$$k_{B_i^0/B_2I}^{eff} = \left(\frac{4 \pi r_{cap} D_B^+ (p/n_i)}{K_{B_i^0/B_2I} C_{I^0}^* (1 + \gamma_{B_i^0/B_2I}^{eff})} \right), \quad (26)$$

$$\gamma_{B_i^-/B_2I}^{eff} = D_B^0 / (D_{I^0} C_{I^0}^* K_{I^0/(B_i)^-} - K_{B_i^-/B_2I}), \quad (27)$$

$$\gamma_{B_i^0/B_2I}^{eff} = D_B^+ / (D_{I^0} C_{I^0}^* K_{I^0/(B_i)^0} + K_{B_i^0/B_2I}). \quad (28)$$

The formation of $(BI_2)^+$ can proceed by these reactions,



The overall net reaction rate is thus

TABLE III. Cluster equilibrium constants after optimization in the simple model including charge state effects.

Parameter	Eq. No.	Prefactor	E_{BI} (eV)
$K_{(B_i)^-/B^-,I^0}$		2×10^{-23}	0.93
$K_{(B_i)I^0}$	15	2×10^{-23}	1.2
$K_{(B_i)^-/B_2I}$	18	1.66×10^{-19}	4.7
$K_{(B_i)I^+}$	28	2×10^{-23}	1.22

$$R_{BI_2} = k_{BI_2} \left[C_{(B_i)I^+} C_{I^+} - \frac{C_{BI_2}}{K_{(B_i)I^+}} \right], \quad (33)$$

$$k_{BI_2} = 4 \pi a (D_{B_i} + D_I) \left(1 + \frac{1}{K_{I^+}} \frac{n}{n_i} \right) \left(1 + \frac{D_B^0}{D_B^+} \frac{n}{n_i} \right). \quad (34)$$

V. COMPARISON TO DATA

The model parameters for the extended model were optimized to fit a wide range of data including the TED data shown in previous section. Tables II and III tabulate the point defect and boron clustering parameters used for all the simulations shown below. Shown in Fig. 6 is comparison to data from Intel.²⁶ Similarly, Fig. 7 shows comparison to data from Solmi and Baruffaldi.¹² We find the boron cluster model can also predict TED profiles for higher boron doses by including a loop model for interstitials. Shown in Figs. 8 and 9 is comparison to data^{12,26} for $2 \times 10^{15} \text{ cm}^{-2}$, 40 and 20 keV B implants annealed at 800 °C for 1 h. However, it should be noted that this model is not sufficient for high dose, high temperature anneals. For these cases, experiments show sharp boron peaks suggestive of larger sized clusters. We have successfully included larger size clusters to model such data.

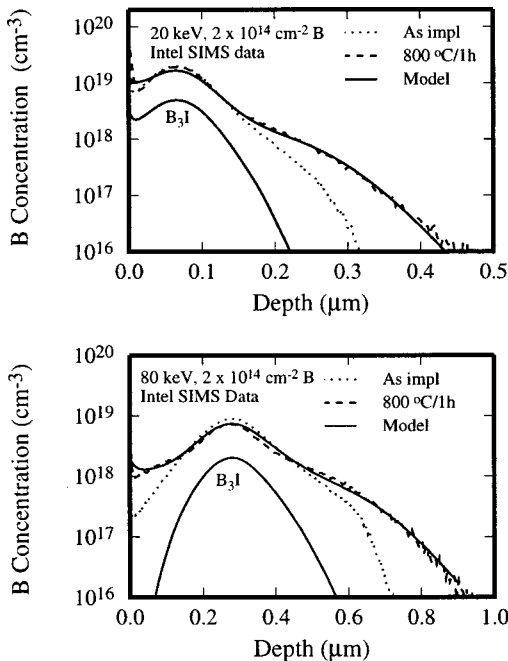


FIG. 6. Comparison of simulation to experimental data for $2 \times 10^{14} \text{ cm}^{-2}$ 20 and 80 keV boron implants after a 1 h anneal at 800 °C. SIMS data from Ref. 26.

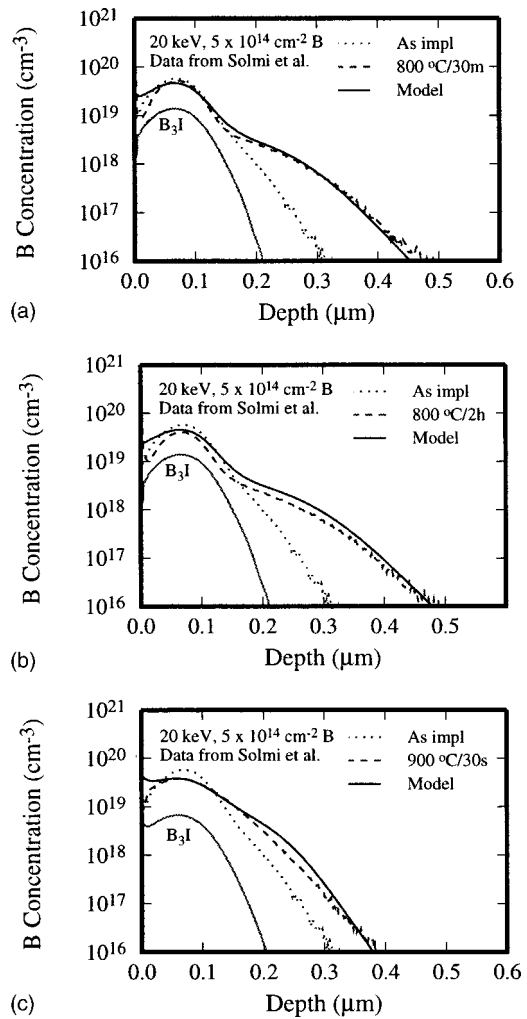


FIG. 7. Comparison of simple model to experimental data for a $5 \times 10^{14} \text{ cm}^{-2}$ B implant annealed at (a) 800 °C for 30 min (b) 800 °C for 2 h (c) 900 °C for 30 s. SIMS data from Ref. 12.

VI. CONCLUSION

We have developed a set of models for predicting boron diffusion subsequent to ion implantation. For medium and low energy boron implants, we have developed a simple cluster model for modeling boron interstitial clusters. This system was derived from a multicluster model based on *ab*

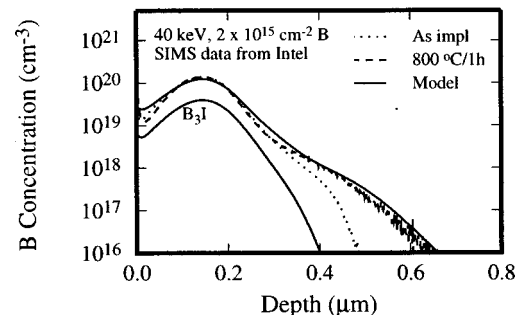


FIG. 8. Comparison of simulation to experimental data for a $2 \times 10^{15} \text{ cm}^{-2}$ 40 keV boron implant after a 1 h anneal at 800 °C. SIMS data is from Ref. 26.

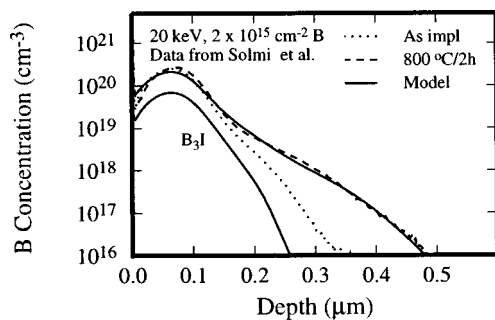


FIG. 9. Comparison of model to experimental data for a $2 \times 10^{15} \text{ cm}^{-2}$, 20 keV B implant annealed at 800 °C. SIMS data is from Ref. 12.

initio calculations performed at Lawrence Livermore National Labs.¹⁷ Based on analysis of cluster kinetics and energetics, we are able to match the results of the full multicluster model, while reducing the number of cluster continuity equations from ten to just two. The resulting model clearly illuminates the critical processes involved in boron clustering. We further extended this model to include the presence of charged cluster species, and characterized the model parameters based on experimental results. Despite its simplicity, the model accurately describes boron clustering and anomalous diffusion over a range of experimental conditions.

ACKNOWLEDGMENTS

The authors would like to thank M. Giles of Intel, S. Solmi of CNR-LAMEL, and H. Gossmann of Lucent for details and discussion regarding their experimental results. This work was supported by the Semiconductor Research Corporation.

¹N. E. B. Cowern, K. T. F. Janssen, and H. F. F. Jos, *J. Appl. Phys.* **68**, 6191 (1990).

²P. A. Packan and J. D. Plummer, *Appl. Phys. Lett.* **56**, 1787 (1990).

³M. Yoshida, *Jpn. J. Appl. Phys.* **18**, 479 (1979).

- ⁴M. Yoshida, *Jpn. J. Appl. Phys., Part 1* **22**, 1404 (1983).
- ⁵D. Mathiot and J. C. Pfister, *J. Appl. Phys.* **53**, 3035 (1982).
- ⁶D. Mathiot and J. C. Pfister, *J. Appl. Phys.* **55**, 3518 (1984).
- ⁷D. J. Eaglesham, P. A. Stolk, H. J. Gossmann, and J. M. Poate, *Appl. Phys. Lett.* **65**, 2305 (1994).
- ⁸D. J. Eaglesham, P. A. Stolk, H. J. Gossmann, T. E. Haynes, and J. M. Poate, *Nucl. Instrum. Methods Phys. Res. B* **106**, 191 (1995).
- ⁹N. E. B. Cowern, G. F. A. van de Walle, P. C. Zalm, and D. W. E. Vandenhout, *Appl. Phys. Lett.* **65**, 2981 (1994).
- ¹⁰K. S. Jones, J. Lui, L. Zhang, V. Krishnamoorthy, and R. T. DeHoff, *Nucl. Instrum. Methods Phys. Res. B* **106**, 227 (1995).
- ¹¹J. Lui, M. E. Law, and K. S. Jones, *Solid-State Electron.* **38**, 1305 (1995).
- ¹²S. Solmi and F. Baruffaldi, *J. Appl. Phys.* **69**, 2135 (1991).
- ¹³A. H. Gencer, S. Chakravarthi, and S. T. Dunham, *Proceedings of the International Conference on Simulation of Semiconductor Processes and Devices* (IEEE, New York, 1997), p. 77.
- ¹⁴L. Pelaz, M. Jaraiz, G. H. Gilmer, H. J. Gossmann, C. S. Rafferty, and D. J. Eaglesham, *Appl. Phys. Lett.* **70**, 2285 (1997).
- ¹⁵A. D. Lilak, S. K. Earles, K. S. Jones, M. E. Law, and M. D. Giles, *Proceedings of the International Electron Device Meeting* (IEEE, New York, 1997), p. 493.
- ¹⁶S. Chakravarthi and S. T. Dunham, *Proceedings of the International Conference on Simulation of Semiconductor Processes and Devices* (Springer, Wien, 1998), p. 55.
- ¹⁷M. J. Caturla, M. D. Johnson, and T. D. de la Rubia, *Appl. Phys. Lett.* **72**, 2736 (1998).
- ¹⁸F. Wittel, PhD thesis, Boston University, 1995.
- ¹⁹M. Jaraiz, G. H. Gilmer, J. M. Poate, and T. D. de la Rubia, *Appl. Phys. Lett.* **68**, 409 (1996).
- ²⁰S. Chakravarthi and S. T. Dunham, *Mater. Res. Soc. Symp. Proc.* **469**, 47 (1997).
- ²¹M. Tang, J. Zhu, and T. Diaz de la Rubia, *Phys. Rev. B* **55**, 14 279 (1997).
- ²²H. Bracht, N. A. Stolwijk, and H. Mehrer, *Phys. Rev. B* **52**, 16 542 (1995).
- ²³M. D. Giles, *J. Electrochem. Soc.* **138**, 1160 (1991).
- ²⁴A. H. Gencer and S. T. Dunham, *J. Appl. Phys.* **81**, 631 (1997).
- ²⁵A. H. Gencer, PhD thesis, Boston University, 1999.
- ²⁶M. D. Giles, TED SIMS data from Intel Corporation.
- ²⁷L. Pelaz, G. H. Gilmer, H.-J. Gossmann, C. S. Rafferty, M. Jaraiz, and J. Barbolla, *Appl. Phys. Lett.* **74**, 3657 (1999).
- ²⁸H.-J. Gossmann, G. H. Gilmer, C. S. Rafferty, F. C. Unterwald, T. Boone, J. M. Poate, H. S. Luftman, and W. Frank, *J. Appl. Phys.* **77**, 1948 (1995).
- ²⁹T. J. Lenosky, S. K. Theiss, and T. D. de la Rubia (private communication).
- ³⁰W. Windl, M. M. Bunea, R. Stumpf, S. T. Dunham, and M. P. Masquelier, *Phys. Rev. Lett.* **83**, 4345 (1999).
- ³¹M. D. Giles, *IEEE Trans. CAD* **8**, 460 (1989).